

The Pre-He White Dwarfs in Eclipsing Binaries. IV. WASP 1814+48 with Multiperiodic Pulsations

Jae Woo Lee^{1*}, Kyeongsoo Hong², Hye-Young Kim³ and Jang-Ho Park¹

¹*Korea Astronomy and Space Science Institute, Daejeon 34055, Republic of Korea*

²*Institute for Astrophysics, Chungbuk National University, Cheongju 28644, Republic of Korea*

³*Department of Astronomy and Space Science, Chungbuk National University, Cheongju 28644, Republic of Korea*

Accepted 2022 ———. Received 2022 ———; in original form 2022

ABSTRACT

For the EL CVn candidate 1SWASPJ181417.43+481117.0 (WASP 1814+48), we secured the first spectroscopic observations between 2015 April and 2021 March. Using the echelle spectra, the radial velocities (RVs) of the primary star were measured with its atmospheric parameters of $T_{\text{eff},1} = 7770 \pm 130$ K and $v_1 \sin i = 47 \pm 6$ km s⁻¹. We fitted our single-lined RVs and the TESS light curve simultaneously. From the binary modeling, we determined the following fundamental parameters for each component: $M_1 = 1.659 \pm 0.048 M_{\odot}$, $R_1 = 1.945 \pm 0.027 R_{\odot}$, and $L_1 = 12.35 \pm 0.90 L_{\odot}$ for WASP 1814+48 A, and $M_2 = 0.172 \pm 0.005 M_{\odot}$, $R_2 = 0.194 \pm 0.005 R_{\odot}$, and $L_2 = 0.69 \pm 0.07 L_{\odot}$ for WASP 1814+48 B. The surface gravity of $\log g_2 = 5.098 \pm 0.026$ obtained from M_2 and R_2 is concurrent with 5.097 ± 0.025 computed directly from the observable quantities. WASP 1814+48 B is well-matched with the $0.176 M_{\odot}$ white dwarf (WD) evolutionary model for $Z = 0.01$. The metallicity and our Galactic kinematics indicate that the program target is a thin-disk star. The whole light residuals after removal of the binary trend were analyzed and found to oscillate at a total of 52 frequencies. Among these, most of the low frequencies below 24 day^{-1} are aliases and orbital harmonics. The five significant frequencies between 32 and 36 day^{-1} are the pulsation modes of WASP 1814+48 A located in the δ Sct domain on ZAMS, and the high frequencies of 128 – 288 day^{-1} arise from WASP 1814+48 B in the pre-He WD instability strip. Our results reveal that WASP 1814+48 is the fifth EL CVn star that is composed of a δ Sct-type primary and a pre-ELMV (extremely low-mass pre-He WD variable).

Key words: binaries: eclipsing - binaries: spectroscopic - stars: fundamental parameters - stars: individual (1SWASPJ181417.43+481117.0) - stars: oscillations (including pulsations).

1 INTRODUCTION

Extremely low-mass ($\lesssim 0.3 M_{\odot}$) white dwarfs (ELM WDs) are the remnants of stars that cannot burn helium (He) in their cores. Because the Universe does not have enough time to produce them by single-star evolution, the He-core ELM WDs are thought to be formed by considerable mass loss at the red giant branch phase of stellar binaries before He burning (Marsh, Dhillon & Duck 1995; Kilic, Stanek & Pinsonneault 2007). In this case, they can provide information about the past evolution of the precursor binaries. We have been performing time-series spectroscopy on eclipsing binaries (EBs) containing an ELM WD precursor (pre-ELM WD) as possible (Lee et al. 2020). The main purpose of the observations is to measure the fundamental parameters of the interesting rare objects, combining existing or new photometric data, and to present their evolution scenario. The promising targets for this subject are EL CVn-type binaries, which are post-mass transfer stars comprising an A/F main sequence and a pre-ELM WD companion (Maxted et al. 2014; van Roestel et al. 2018).

Five out of ~ 70 EL CVn stars are pulsating EBs that exhibit possible multiperiodic oscillations arising from both a δ Sct (or γ Dor)-type primary and a pre-ELMV companion (Hong et al. 2021; Kim et al. 2021). Because the fundamental parameters such as masses and radii can be measured accurately and in detail, spectroscopic and eclipsing binaries provide us

* E-mail: jwlee@kasi.re.kr

with an opportunity to test and refine the evolutionary models of stars (Hilditch 2001; Torres, Andersen & Giménez 2010). At the same time, pulsating stars help to probe and constrain their interior physics from core to surface through asteroseismology (Antoci et al. 2019; Aerts 2021). Thus, the stellar pulsations in EBs are of great value, because the synergy between the two kinds of variables can clearly enhance our understanding of stellar physics (Murphy 2018; Kurtz 2022).

We focus on the EL CVn-type star 1SWASPJ181417.43+481117.0 (WASP 1814+48; TIC 420947520; Gaia EDR3 2122136709525411072), which was recognized by Maxted et al. (2014) to be an eclipsing variable with a period of 1.7994305 ± 0.0000005 days. From archival WASP photometry, they found that the binary target is a totally-eclipsing detached system with a mass ratio of $q = 0.134 \pm 0.015$, relative radii of $r_1 = 0.2565 \pm 0.0025$ and $r_2 = 0.0247 \pm 0.0004$, and surface brightness and luminosity ratios of $J = 3.000 \pm 0.064$ and $L_2/L_1 = 0.0277 \pm 0.0002$, respectively. Further, the effective temperatures of the brighter, more massive primary star and its companion were obtained to be 8000 ± 300 K and $12,500 \pm 1800$ K, respectively, by comparing the observed and synthetic flux distributions. This work is the fourth in a paper-series on the pre-ELM WDs in EBs (Lee et al. 2020; Lee, Hong & Park 2022; Hong et al. 2021). We analyze in detail our high-resolution spectra and the TESS photometric data of WASP 1814+48, and report the discovery of multiple types of pulsations originating from the EB system.

2 TESS PHOTOMETRY AND ECLIPSE TIMINGS

Highly precise photometry of WASP 1814+48 has been performed by the TESS mission (Ricker et al. 2015) from 2019 July 18. We downloaded the 2-min cadence data taken during Sector 14, 25-26, and 40-41 from MAST¹ and used the simple aperture photometry (SAP_FLUX) data in this study. The flux measurements were detrended and normalized by fitting a second-order polynomial to the out-of-eclipse portion of each sector’s light curve, and they were converted to magnitude units. The resultant observations are displayed in the top panel of Figure 1. A total of 91,240 individual points were obtained for the five sectors. The crowdedness factor CROWDSAP reported in the TESS data is the ratio of the target flux to the total flux in a photometric aperture. This can be used to see if nearby stars are observed in the same pixel as the target, where a value of 1 means that there is no contamination. The CROWDSAP value for WASP 1814+48 is 0.9900 ± 0.0024 on average for these sectors.

The TESS eclipse times of WASP 1814+48 and their errors were determined using the Kwee & van Woerden (1956) method. These are presented in Table 1, where Min I and II present the primary and secondary eclipses, respectively, at orbital phases 0.0 and 0.50. In order to obtain the updated linear ephemeris of the binary star and to phase its time-series data, we used the primary minimum epochs in the following least-squares solution:

$$\text{Min I} = \text{BJD } 2, 459, 010.506694(27) + 1.79943078(17)E. \quad (1)$$

The 1σ -error values for each coefficient are given in the parentheses. The timing residuals from the linear ephemeris appear as $O - C$ in Table 1. The TESS light curve phased with Equation (1) is depicted in the middle panel of Figure 1.

3 GROUND-BASED SPECTROSCOPY AND DATA ANALYSIS

The spectroscopic observations of WASP 1814+48 were performed with the Bohyunsan Observatory Echelle Spectrograph (BOES; Kim et al. 2007), attached to the 1.8-m telescope in the Bohyunsan Optical Astronomy Observatory (BOAO), Korea. A total of 31 spectra were secured for seven nights between 2015 April and 2021 March. Their wavelength coverage ranges from 3600 to 10,200 Å with a resolving power of $R = 30,000$. Each exposure time of our target star was 40 min, resulting in a signal-to-noise (S/N) ratio of approximately 20 around 4500 Å. This corresponds to 0.015 of the eclipsing period, so orbital smearing was not considered. All observed spectra were reduced by following the IRAF standard data-reduction procedures (Hong et al. 2015), which include flat fielding, de-biasing, extraction, and wavelength and flux calibration.

Figure 2 shows the trailed spectra of WASP 1814+48 in the Mg II $\lambda 4481$ region. In this figure, the S-wave feature of the more massive primary component (WASP 1814+48 A) is clearly shown, while there is no sign of the hotter secondary star (WASP 1814+48 B). To measure the radial velocities (RVs) from the observed spectra, we used the cross-correlation function (CCF) method (Simkin 1974; Tonry & Davis 1979) implemented in the RaveSpan software (Pilecki, Konorski & Gorski 2012; Pilecki et al. 2017). In the run, most of metallic and Balmer lines are difficult to measure, so we selected the spectral region of Mg II $\lambda 4481$ that is useful for determining the RVs of the EL CVn-type stars (Lee et al. 2020 for WASP 0131+28; Hong et al. 2021 for WASP 0843-11; Lee, Hong & Park 2022 for WASP 1625-04). Template spectra were taken from the BOSZ stellar atmosphere models² (Bohlin et al. 2017) matching the effective temperature ($T_{\text{eff},1}$) and surface gravity ($\log g_1$) of the primary component discussed below. We measured the RVs of WASP 1814+48 A and they are presented in Figure 3 and Table 2. The RV measurements were fitted to a sine wave (Lee et al. 2018), in order to obtain the spectroscopic orbit of WASP 1814+48 A. The results from this calculation are summarized in Table 3, where γ is the systemic velocity, K_1 and $a_1 \sin i$ are the velocity semi-amplitude and semimajor axis of the primary component, and $f(M)$ is the mass function. The orbital period $P = 1.79943078$ days was taken from Eq. (1).

¹ <https://archive.stsci.edu/>

² <https://archive.stsci.edu/prepds/bosz>

To determine the rotational velocities ($v_1 \sin i$) and surface temperature ($T_{\text{eff},1}$) of WASP 1814+48 A, we selected five absorption lines, Ca II K $\lambda 3933$, H $_{\gamma}$ $\lambda 4340$, Fe II $\lambda 4383$, H $_{\beta}$ $\lambda 4861$, and H $_{\alpha}$ $\lambda 6563$, which are useful spectral indicators for A0–F0 type stars (Gray & Corbally 2009). From the BOES spectra, each absorption region was combined using the FDBINARY code (Ilijic et al. 2004) to obtain a better S/N spectrum. Maxted et al. (2014) estimated the surface temperature of WASP 1814+48 A to be 8000 ± 300 K, based on the surface brightness ratio and the observed flux distribution. Therefore, the reconstructed spectrum was compared to the synthetic spectra with a temperature range of 6500 K–9000 K (in steps of 10 K) and the projected rotational velocity range of 10–200 km s $^{-1}$ (in steps of 1 km s $^{-1}$). The synthetic spectra were interpolated using the stellar models from the BOSZ spectral library (Bohlin et al. 2017) by adopting the solar metallicity and the surface gravity of $\log g_1 = 4.1$ (cf. Section 4). We obtained both atmospheric parameters of WASP 1814+48 A by performing a χ^2 grid search that minimizes the difference between the synthetic and reconstructed spectra and averaging the values found in each region (Hong et al. 2017; Lee, Hong & Park 2022). As a consequence, $T_{\text{eff},1} = 7770 \pm 130$ K and $v_1 \sin i = 47 \pm 6$ km s $^{-1}$. In Figure 4, the reconstructed spectrum from the FDBINARY code is presented with the best-fit model.

4 BINARY MODELING

As with the archival WASP observations, the TESS light curve of WASP 1814+48 shows a box-shaped primary eclipse and an ellipsoidal variation. The shape resembles that of EL CVn, its class prototype, and there are no noticeable differences between each sector. The observed depths for the primary and secondary eclipses are 0.031 mag and 0.016 mag, respectively, in the TESS photometry, and 0.037 mag and 0.017 mag in the WASP one. In both the WASP and TESS light curves, the phase difference between Min I and Min II implies that WASP 1814+48 is in a circular orbit. To obtain improved binary parameters, we solved the TESS photometric data with our RV curve using the detached mode 2 of the Wilson-Devinney program (Wilson & Devinney 1971; van Hamme & Wilson 2007; hereafter W-D) and applied a mass ratio (q)-search method (e.g., Lee, Hong & Kristiansen 2019). The binary modeling was done in a manner similar to the single-lined eclipsing system HW Vir (Lee et al. 2009) and the EL CVn-type star WASP 0131+28 (Lee et al. 2020).

In the synthesis of the RV and light curves, the surface temperature of WASP 1814+48 A was given as $T_1 = 7700 \pm 130$ K from our spectroscopic analysis, as discussed in the previous section. The albedos (A) and gravity-darkening exponents (g) for both components were all set to 1.0 from their temperatures. The logarithmic limb-darkening (LD) law was adopted and its bolometric (X, Y) and monochromatic (x, y) coefficients were interpolated from the values of van Hamme (1993) incorporated into the W-D program. Because the TESS passband is not included in the binary code, we used the LD parameters for Cousins I_c -band. Furthermore, a circular orbit ($e = 0$) and a synchronous rotation ($F_1 = F_2 = 1.0$) were applied. In this article, WASP 1814+48 A and B are denoted by subscripts 1 and 2, respectively.

The mass ratio is considered the most important parameter in binary modeling. We can directly calculate the velocity semi-amplitudes (K_1 and K_2) and the mass ratio ($q = K_1/K_2$) from double-lined RV curves. However, WASP 1814+48 B was too faint to measure its RVs. Hence, we computed a series of binary models for assumed mass ratios below 0.3, the so-called q -search procedure. The sum of squares of residuals ($\sum W(O - C)^2$) showed a global minimum around $q = 0.104$. The q value was adjusted to obtain the best-fit parameters of the eclipsing system. The final result is presented in Table 4, and the synthetic light and RV curves are displayed as solid curves in the middle panel of Figure 1 and the upper panel of Figure 3, respectively. The residuals between the observations and the binary model are plotted in the bottom panels of each figure. We can see our modeling result that describes the light and RV curves very well. The parameters' errors in Table 4 were obtained following the method introduced by Southworth et al. (2020) and applied by Lee, Hong & Kim (2021) for the highly-precise TESS data.

The fundamental stellar parameters of WASP 1814+48 A and B were first computed from our simultaneous light and velocity solution. The results are summarized in Table 5. We used the solar temperature and bolometric magnitude of $T_{\text{eff}\odot} = 5780$ K and $M_{\text{bol}\odot} = +4.73$, respectively. The bolometric corrections (BCs) were made using the empirical calibration between $\log T_{\text{eff}}$ and BC presented in Flower (1996) and later corrected in Torres (2010). Using an apparent visual magnitude of $V = 10.673 \pm 0.008$ and the color excess of $E(B - V) = 0.028 \pm 0.007$ (Stassun et al. 2019), we determined the distance of the target star to be 536 ± 20 pc. Within 3σ -error values, our distance coincides with 586 ± 5 pc inverted from the GAIA EDR3 parallax of 1.706 ± 0.013 mas (Gaia Collaboration et al. 2021) and 584 ± 4 pc estimated from the GAIA EDR3 measurements by Bailer-Jones et al. (2021).

The synchronous rotations for the component stars were calculated to be $v_{1,\text{sync}} = 54.70 \pm 0.77$ km s $^{-1}$ and $v_{2,\text{sync}} = 5.46 \pm 0.15$ km s $^{-1}$ from the binary period P and their radii $R_{1,2}$. Since both values of $v_{1,\text{sync}}$ and $v_1 \sin i$ coincide close to the margins of errors, we believe the primary star is currently in a state of synchronized rotation or nearly so.

5 PULSATONAL CHARACTERISTICS

The physical parameters of WASP 1814+48 in Table 5 indicate that the primary and secondary components are δ Sct and pre-ELMV candidates, respectively (Maxted et al. 2013; Wang, Zhang & Dai 2020; Hong et al. 2021). To find the pulsation signatures present in the TESS observations, we applied a multifrequency analysis to the entire light curve residuals from our binary model. The PERIOD04 software of Lenz & Breger (2005) was conducted up to the Nyquist limit of about 360 day $^{-1}$. The periodogram for WASP 1814+48 is presented in Figure 5, where two dominant signals are clearly visible around 33 day $^{-1}$.

In addition, as shown in the inset box, there are the orbital frequency ($f_{\text{orb}} = 0.55573 \text{ day}^{-1}$) and its multiples (Nf_{orb} , N is an integer) in the low-frequency domain. We performed an iterative pre-whitening process (Lee et al. 2014), and extracted 52 frequencies with an S/N amplitude ratio larger than about 4.0 (Breger et al. 1993). The results of this process are summarized in Table 6, and the uncertainties of each parameter were computed following the method proposed by Kallinger, Reegen & Weiss (2008). The amplitude spectra after pre-whitening the first two frequencies and then 38 frequencies are illustrated in the middle and bottom panels of Figure 5, respectively.

Of the extracted signals, possible orbital harmonics and combination frequencies were carefully examined using the frequency resolution of $\Delta f \simeq 0.002 \text{ day}^{-1}$ (Loumos & Deeming 1978). They are remarked in the last column of Table 6. Most frequencies lower than 24 day^{-1} may be either alias effects or orbital harmonics up to $42f_{\text{orb}}$. The integer multiples of the orbital frequency can arise from tidally excited pulsations by the companions in eccentric binary systems such as the heartbeat star KOI-54 (Welsh et al. 2011). However, our binary model favors the conclusion that WASP 1814+48 is in a circular orbit. Thus, it is difficult to regard the observed multiples of Nf_{orb} as stellar oscillations excited by tidal interaction. We think the aliases and the orbital harmonics result from insufficient removal of the binary effects and the systematic trends in the TESS data.

To cross-check the significant frequencies found from the entire TESS observations and to examine their variations with time, we independently analyzed the light curve residuals of each sector in the same way as before. The resultant frequencies were compared with those in Table 6. Only f_1 , f_2 , f_6 , and f_9 were detected in all sectors, and f_{11} in all but Sector 14. The five frequencies were stable within the standard deviation of $\sim 0.002 \text{ day}^{-1}$. The remaining frequencies except for some orbital harmonics (f_{orb} , $2f_{\text{orb}}$, $3f_{\text{orb}}$) were not found in most sectors. On the other hand, if the high frequencies between 128 and 288 day^{-1} result from WASP 1814+48 B with about 2% light contribution to the EB system, they are highly diluted by the light of WASP 1814+48 A. Then, these signals would have been too weak to detect in each sector with the frequency resolution of $\sim 0.055 \text{ day}^{-1}$. As the pre-He WD transits the larger and more massive primary star during the secondary eclipses, we analyzed the entire secondary-eclipse residuals (orbital phases 0.454–0.546). The primary-eclipse data were also analyzed for comparison. Figure 6 presents the amplitude spectra of both eclipse phases in the frequency region of 100–300 day^{-1} . Two high-frequency signals of 127.2627 and 135.5987 day^{-1} were detected only in the secondary eclipse phase. This implies that the main source of the high frequencies is the secondary companion WASP 1814+48 B.

6 DISCUSSION AND CONCLUSIONS

It is known from archival WASP photometry (Maxted et al. 2014) that WASP 1814+48 is a candidate EL CVn star. For the target star, we obtained the first spectroscopic observations using the BOES echelle spectrograph attached to the BOAO 1.8-m reflector. From the total 31 spectra, the RVs and atmospheric parameters of the cooler, more massive primary star were measured, and its surface temperature and rotation velocity were determined to be $T_{\text{eff},1} = 7770 \pm 130 \text{ K}$ and $v_1 \sin i = 47 \pm 6 \text{ km s}^{-1}$, respectively. The spectroscopic measurements were solved with the high-precision photometric data from the TESS mission. The combined solution demonstrates that WASP 1814+48 is an EL CVn-type detached EB with masses of $M_1 = 1.659 \pm 0.048 M_{\odot}$ and $M_2 = 0.172 \pm 0.005 M_{\odot}$, radii of $R_1 = 1.945 \pm 0.027 R_{\odot}$ and $R_2 = 0.194 \pm 0.005 R_{\odot}$, and luminosities of $L_1 = 12.35 \pm 0.90 L_{\odot}$ and $L_2 = 0.69 \pm 0.07 L_{\odot}$. The component stars fill $f_1 = 49\%$ and $f_2 = 36\%$ of their inner Roche lobe, respectively.

The surface gravity of the secondary companion can be calculated directly from the light and RV parameters without knowledge of its mass and radius (Southworth, Wheatley & Sams 2007) and is represented as:

$$g_2 = \frac{GM_2}{R_2^2} = \frac{2\pi K_1(1-e^2)^{1/2}}{P r_2^2 \sin i} \quad (2)$$

The observable quantities of P , r_2 , i and K_1 were taken from Table 4. This calculation results in $\log g_2 = 5.097 \pm 0.025$, which is well-matched with the 5.098 ± 0.026 obtained from the secondary's mass and radius presented in this article.

Following the solar values³ and the procedure applied by Lee et al. (2020), the Galactic space motion of WASP 1814+48 was computed from our system velocity (γ) and the GAIA EDR3 measurements (position, parallax, and proper motion). The obtained velocity components were $U = -18.4 \pm 0.3 \text{ km s}^{-1}$, $V = 252.8 \pm 0.6 \text{ km s}^{-1}$, and $W = 9.1 \pm 0.3 \text{ km s}^{-1}$, which correspond to a total space velocity of $253.6 \pm 0.8 \text{ km s}^{-1}$. Also, the Galactic orbit's eccentricity and angular momentum in the z direction were obtained to be $e_G = 0.1813 \pm 0.0003$ and $J_z = 1980 \pm 17 \text{ kpc km s}^{-1}$, respectively. The position of WASP 1814+48 B in the $U - V$ and $J_z - e_G$ planes falls within the thin-disk population described by Pauli et al. (2006), indicating that our program target has the kinematics of thin-disk stars.

Using the fundamental stellar parameters of WASP 1814+48, we studied the evolutionary history of the EB system in terms of the H-R and $\log T_{\text{eff}} - \log g$ diagrams. The locations of the primary (A) and secondary (B) stars are presented as star symbols in Figure 7, while the oblique dash-dotted and dashed lines denote the instability strips of γ Dor and δ Sct variables. WASP 1814+48 A resides inside the δ Sct region on the ZAMS, which implies that it is a δ Sct candidate. In both diagrams, the black dotted, dashed, and solid lines represent the evolutionary sequences of He-core WD stars with metallicities of $Z = 0.001$, 0.01 , and 0.02 , respectively, for masses of $M = 0.182 M_{\odot}$, $0.176 M_{\odot}$, and $0.171 M_{\odot}$ (Istrate et al. 2016). We can

³ ($X_{\odot}, Y_{\odot}, Z_{\odot}$) = (−8.0, 0.0, 0.0) kpc and ($U_{\odot}, V_{\odot}, W_{\odot}$) = (9.58, 10.52, 7.01) km s^{-1}

see that WASP 1814+48 B with $0.172 \pm 0.005 M_{\odot}$ is in good agreement with the $0.176 M_{\odot}$ WD model for $Z = 0.01$. The result matches well with the thin-disk population classified by our Galactic kinematics. The lifetime (t) of the binary star in a constant luminosity phase was estimated to be about 1.2×10^9 yr using the $M_{\text{WD}} - t$ relation (Chen et al. 2017).

The whole light residuals from our binary model were analyzed using the software Period04 to find multiperiodic frequencies in our target star. We found two dominant oscillations at $f_1 = 33.70479 \text{ day}^{-1}$ and $f_2 = 32.80546 \text{ day}^{-1}$, corresponding to about 42.7 min and 43.9 min, respectively. As a consequence of the pre-whitening process, WASP 1814+48 oscillated in a total of 52 frequencies that satisfied our criterion of $S/N \gtrsim 4.0$. Most signals in the low frequency region of $< 24 \text{ day}^{-1}$ may be sidelobes due to incomplete binary modeling and instrumental artifacts in the TESS observations, but not tidally excited modes and γ Dor pulsations. The five frequencies between 32 and 36 day^{-1} originated from WASP 1814+48 A located in the δ Sct instability domain, as shown in Figure 7. From the pulsation frequency-density relation of $Q_i = f_i \sqrt{\rho/\rho_{\odot}}$, we determined their pulsation constants to be $Q_1 = 0.014$ days, $Q_2 = 0.014$ days, $Q_6 = 0.015$ days, $Q_9 = 0.013$ days, and $Q_{11} = 0.014$ days in pressure (p) modes of δ Sct type with $Q < 0.04$ days (Breger 2000; Antoci et al. 2019). Moreover, the period ratios of $P_{\text{pul}}/P_{\text{orb}} = 0.0155 \sim 0.0171$ are within the threshold of 0.09 ± 0.02 for δ Sct EBs pulsating in p modes (Zhang, Luo & Fu 2013). On the other hand, the frequency signals between 128 and 288 day^{-1} may be pulsation modes related to WASP 1814+48 B in the pre-He WD instability strip (Córscico et al. 2019). The periods and pulsation constants for the five high frequencies are in ranges of $5.0 < P_{\text{pul}} < 11.2$ min and $0.017 \leq Q \leq 0.038$ days, respectively. These results make WASP 1814+48 a very promising target for asteroseismology, consisting of a δ Sct-type primary and a pulsating pre-He WD companion.

ACKNOWLEDGMENTS

We would like to thank the BOAO staffs for assistance during our spectroscopy. This work includes data collected by the TESS mission, which were obtained from MAST. Funding for the TESS mission is provided by the NASA Explorer Program. This research was supported by the KASI grant 2022-1-830-04. K.H. was supported by the grants 2019R1A2C2085965 and 2020R1A4A2002885 from the National Research Foundation (NRF) of Korea.

DATA AVAILABILITY

The data underlying this article will be shared on reasonable request to the first author.

REFERENCES

- Aerts C., 2021, *RvMP*, 93, 015001
 Antoci V. et al., 2019, *MNRAS*, 490, 4040
 Bailer-Jones C. A. L., Rybizki J., Foesneau M., Demleitner M., Andrae R., 2021, *AJ*, 161, 147
 Bohlin R. C. et al., 2017, *AJ*, 153, 234
 Breger M. et al., 1993, *A&A*, 271, 482
 Breger M., 2000, in Breger M., Montgomery M., eds, *ASP Conf. Ser. Vol. 210, Delta Scuti and Related Stars*. Astron. Soc. Pac., San Francisco, p. 3
 Chen X., Maxted P. F. L., Li J., Han Z., 2017, *MNRAS*, 467, 1874
 Córscico A. H., Althaus L. G., Miller Bertolami M. M., Kepler S. O., 2019, *A&ARv*, 27, 7
 Flower P. J., 1996, *ApJ*, 469, 355
 Gaia Collaboration et al., 2021, *A&A*, 649, A1
 Gray R. O., Corbally C., 2009, *Stellar Spectral Classification*. Princeton Univ. Press, Princeton
 Hilditch R. W., 2001, *An Introduction to Close Binary Stars*. Cambridge Univ. Press, Cambridge
 Hong K. et al., 2015, *AJ*, 150, 131
 Hong K. et al., 2017, *AJ*, 153, 247
 Hong K. et al., 2021, *AJ*, 161, 137
 Ilijć S., Hensberge H., Pavlovski K., Freyhammer L. M., 2004, in Hilditch R., Hensberge H., Pavlovski K., eds, *ASP Conf. Ser. Vol. 318, Spectroscopically and Spatially Resolving the Components of the Close Binary Stars*. Astron. Soc. Pac., San Francisco, p. 111
 Istrate A. G. et al., 2016, *A&A*, 595, A35
 Kallinger T., Reegen P., Weiss W. W., 2008, *A&A*, 481, 571
 Kilic M., Stanek K. Z., Pinsonneault M. H., 2007, *ApJ*, 671, 761
 Kim K.-M. et al., 2007, *PASP*, 119, 1052
 Kim S.-L. et al., 2021, *AJ*, 162, 212
 Kurtz D., 2022, arXiv:2201.11629
 Kwee K. K., van Woerden H., 1956, *Bull. Astron. Inst. Netherlands*, 12, 327
 Lee J. W. et al., 2009, *AJ*, 137, 3181
 Lee J. W., Kim S.-L., Hong K., Lee C.-U., Koo J.-R., 2014, *AJ*, 148, 37

- Lee J. W., Hong K., Koo J.-R., Park J.-H., 2018, *AJ*, 155, 5
Lee J. W., Hong K., Kristiansen M. H., 2019, *AJ*, 157, 17
Lee J. W., Koo J.-R., Hong K., Park J.-H., 2020, *AJ*, 160, 49
Lee J. W., Hong K., Kim H.-Y., 2021, *AJ*, 161, 129
Lee J. W., Hong K., Park J.-H., 2022, *MNRAS*, 511, 654
Lenz P., Breger M., 2005, *Comm. Asteroseismology*, 146, 53
Loumos G. L., Deeming T. J., 1978, *Ap&SS*, 56, 285
Marsh T. R., Dhillon V. S., Duck S. R., 1995, *MNRAS*, 275, 828
Maxted P. F. L. et al., 2013, *Natur*, 498, 463
Maxted P. F. L. et al., 2014, *MNRAS*, 437, 168
Morton D. C., 1991, *ApJS*, 77, 119
Murphy S. J., 2018, preprint (arXiv:1811.12659)
Pauli E.-M., Napiwotzki R., Heber U., Altmann M., Odenkirchen M., 2006, *A&A*, 447, 173
Pilecki B., Konorski P., Gorski M., 2012, in Richards M. T., Hubeny I., eds, *Proc. IAU Symp. 292, From Interacting Binaries to Exoplanets*. Cambridge Univ. Press, Cambridge, p. 301
Pilecki B. et al., 2017, *ApJ*, 842, 110
Ricker G. R. et al., 2015, *JATIS*, 1, 014003
Simkin S. M., 1974, *A&A*, 31, 129
Southworth J., Wheatley P. J., Sams G., 2007, *MNRAS*, 379, L11
Southworth J., Bowman D. M., Tkachenko A., Pavlovski K., 2020, *MNRAS*, 497, L19
Stassun K. G. et al., 2019, *AJ*, 158, 138
Tonry J., Davis M., 1979, *AJ*, 84, 1511
Torres G., 2010, *AJ*, 140, 1158
Torres G., Andersen J., Giménez A., 2010, *A&AR*, 18, 67
van Hamme W., 1993, *AJ*, 106, 209
van Hamme W., Wilson R. E., 2007, *ApJ*, 661, 1129
van Roestel J. et al., 2018, *MNRAS*, 475, 2560
Wang K., Zhang X., Dai M., 2020, *ApJ*, 888, 49
Welsh W. F. et al., 2011, *ApJS*, 197, 4
Wilson R. E., Devinney E. J., 1971, *ApJ*, 166, 605
Zhang X. B., Luo C. Q., Fu J. N., 2013, *ApJ*, 777, 77

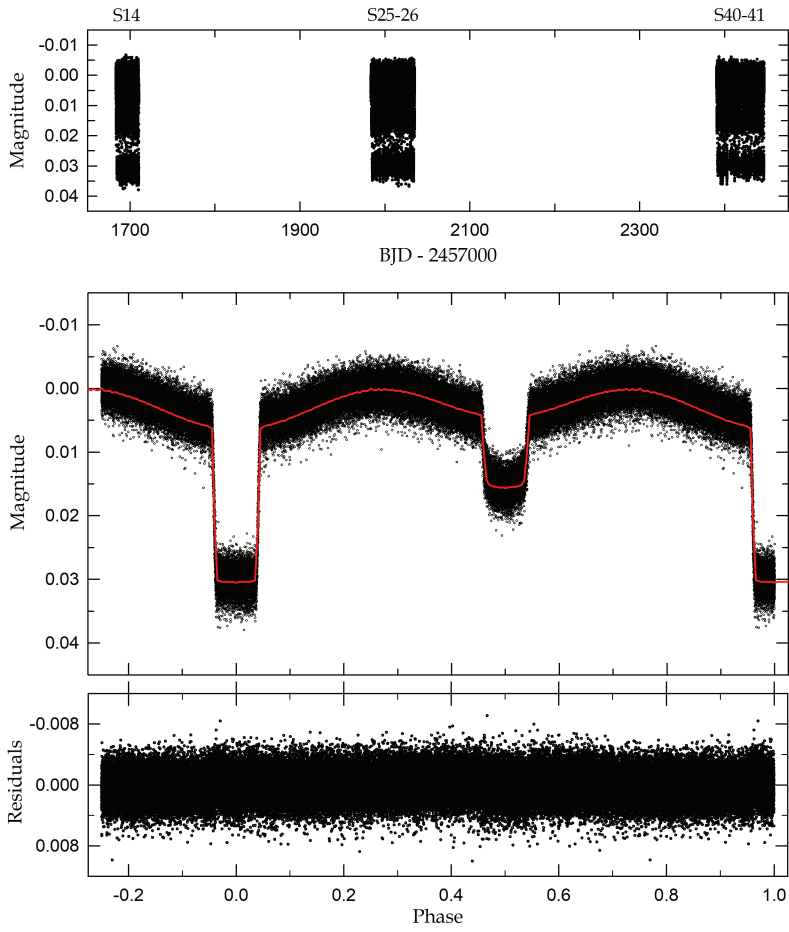


Figure 1. TESS observations of WASP 1814+48 distributed in BJD (top panel) and orbital phase (middle panel). The circles are individual measures and the solid line represents the synthetic curve obtained with our binary model. The corresponding residuals are plotted in the bottom panel.

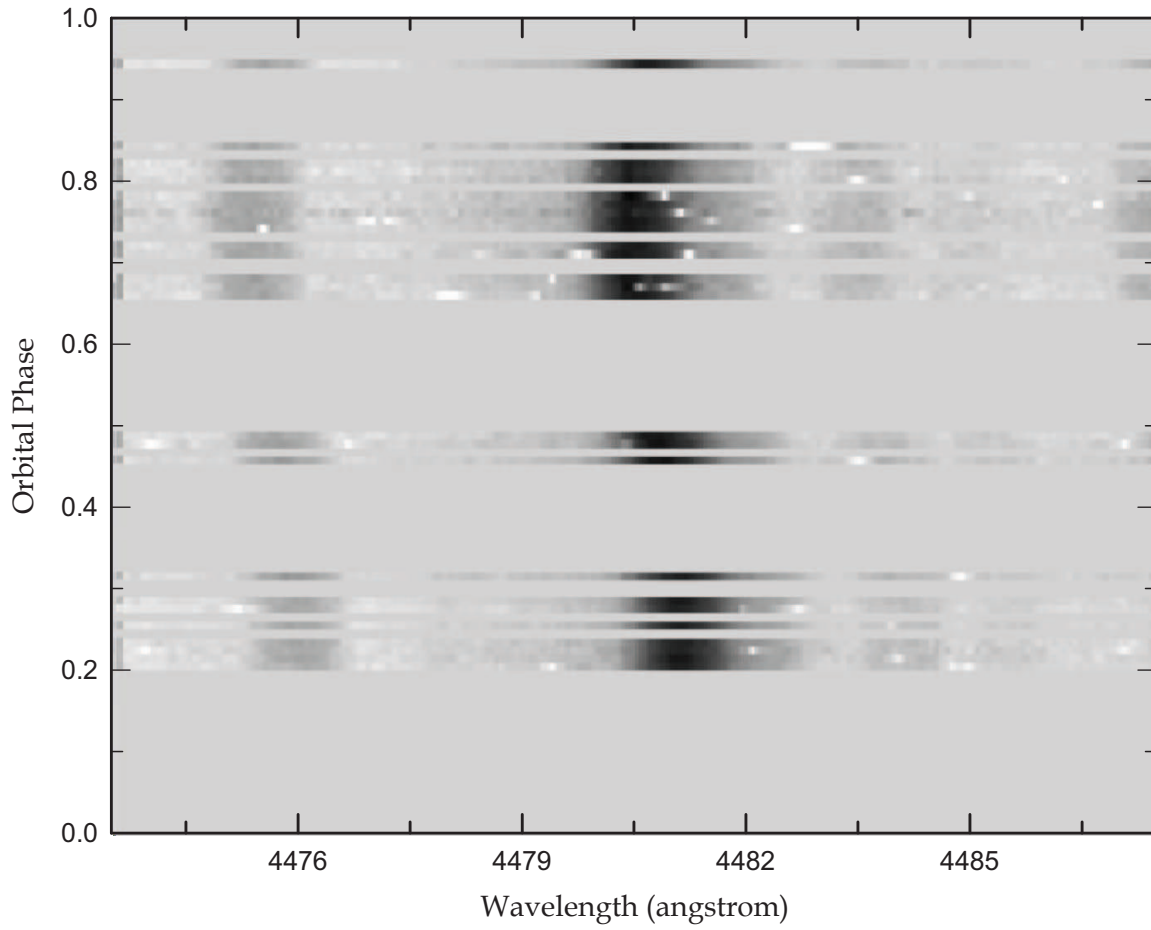


Figure 2. Phase-folded trailed spectra of WASP 1814+48 in the Mg II λ 4481 region.

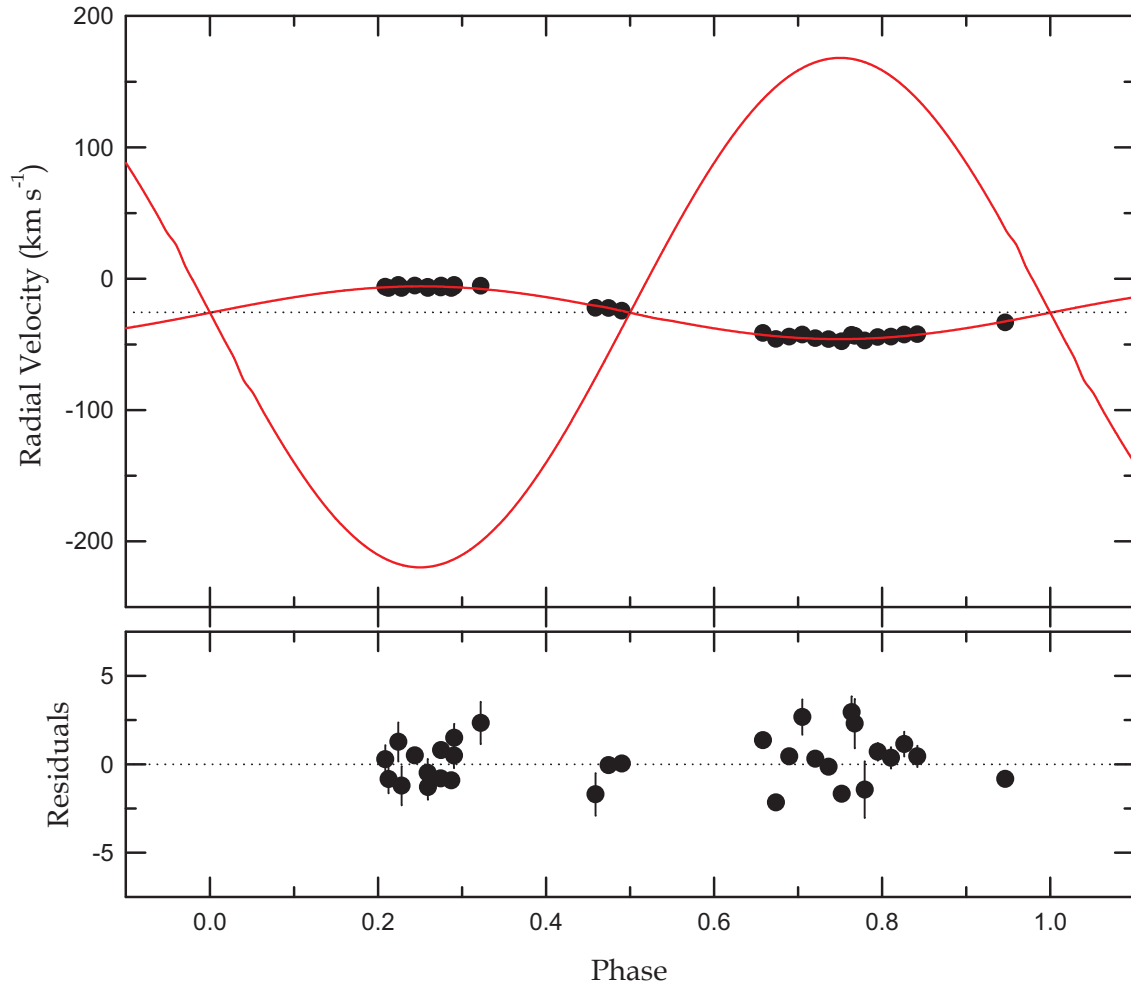


Figure 3. Radial velocities of WASP 1814+48 with a fitted model. The solid curves represent the results from a consistent light and RV curve analysis and the dotted line denotes the system velocity of -25.65 km s^{-1} . The lower panel displays the residuals between measurements and models.

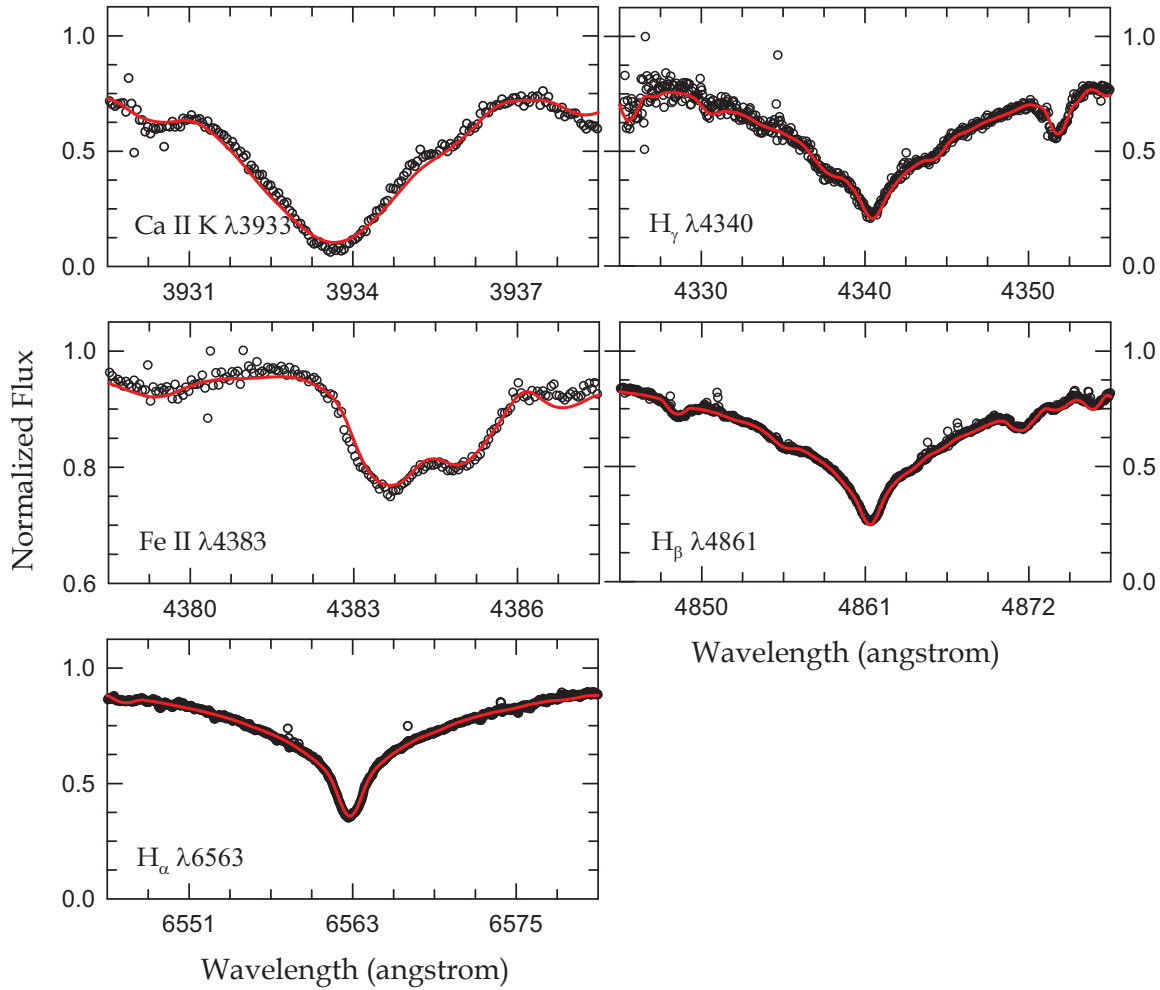


Figure 4. Five spectral regions of WASP 1814+48 A. The open circles and the red lines represent the reconstructed spectrum obtained with the FDBINARY code and the synthetic model spectrum with the best-fitting parameters of $T_{\text{eff},1} = 7770 \pm 130$ K and $v_1 \sin i = 47 \pm 6$ km s $^{-1}$, respectively. The spectra were converted from vacuum to air wavelengths using the IAU standard conversion (Morton 1991).

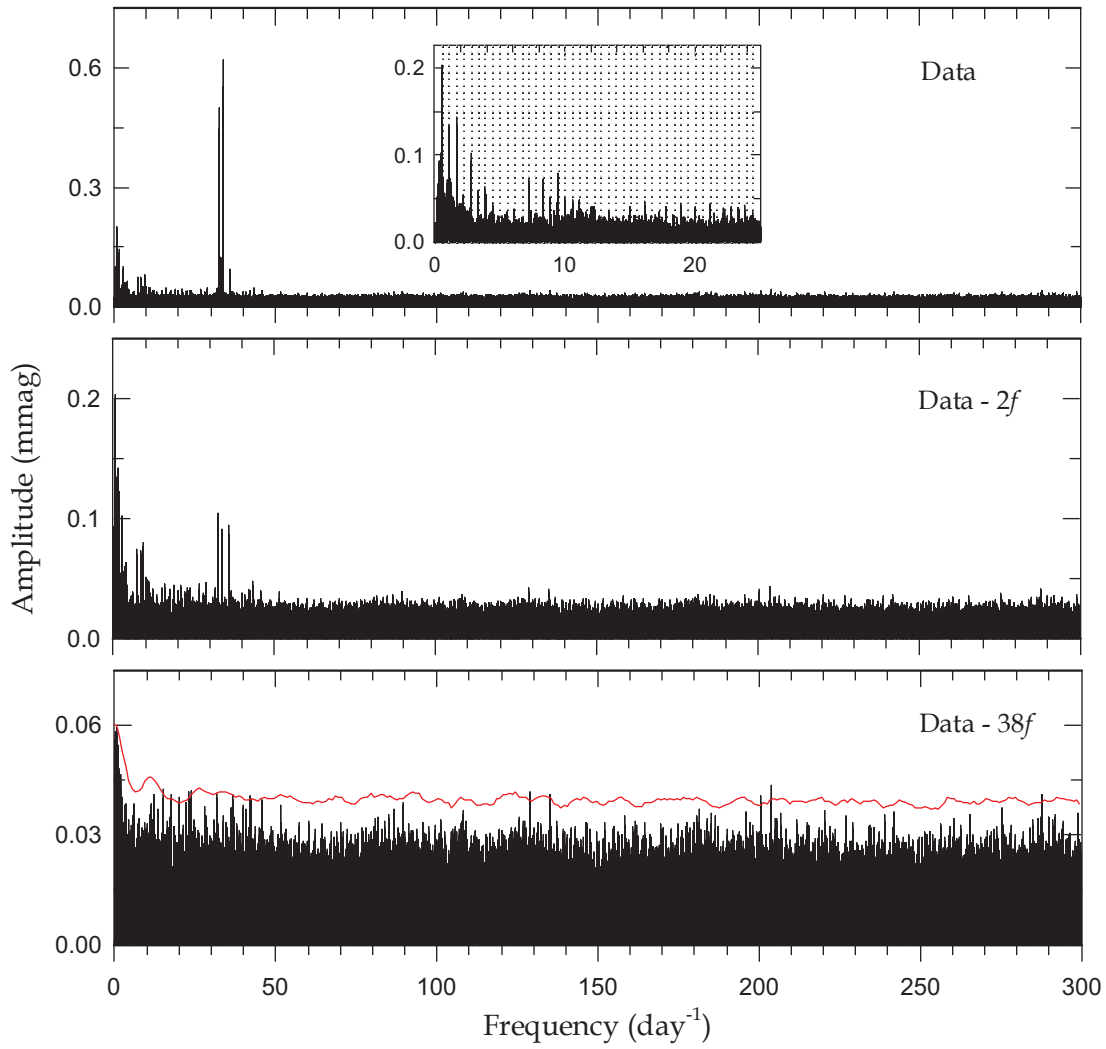


Figure 5. Periodogram from the PERIOD04 program for the entire light curve residuals. The amplitude spectra before and after prewhitening the first two frequencies, and then 38 frequencies are shown in the top to bottom panels. The inset box in the top panel is the amplified spectrum of the low-frequency domain showing a series of orbital harmonics denoted by the vertical dotted lines. The red line in the bottom panel corresponds to four times the noise spectrum.

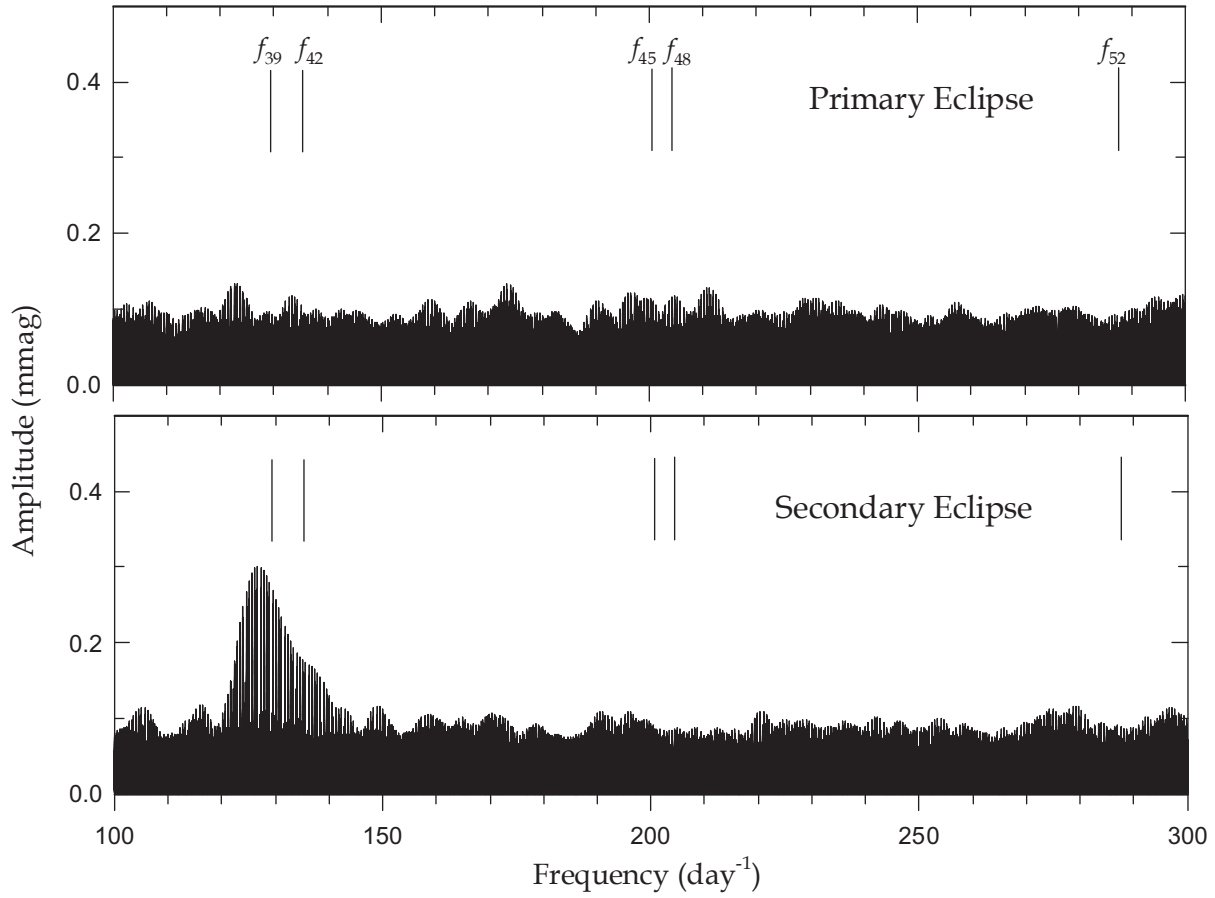


Figure 6. Amplitude spectra for the light curve residuals during times of the primary (upper panel) and secondary (lower panel) eclipses. In both panels, the five vertical lines denote the pulsation frequencies of f_{39} , f_{42} , f_{45} , f_{48} , and f_{52} found from the entire data listed in Table 6.

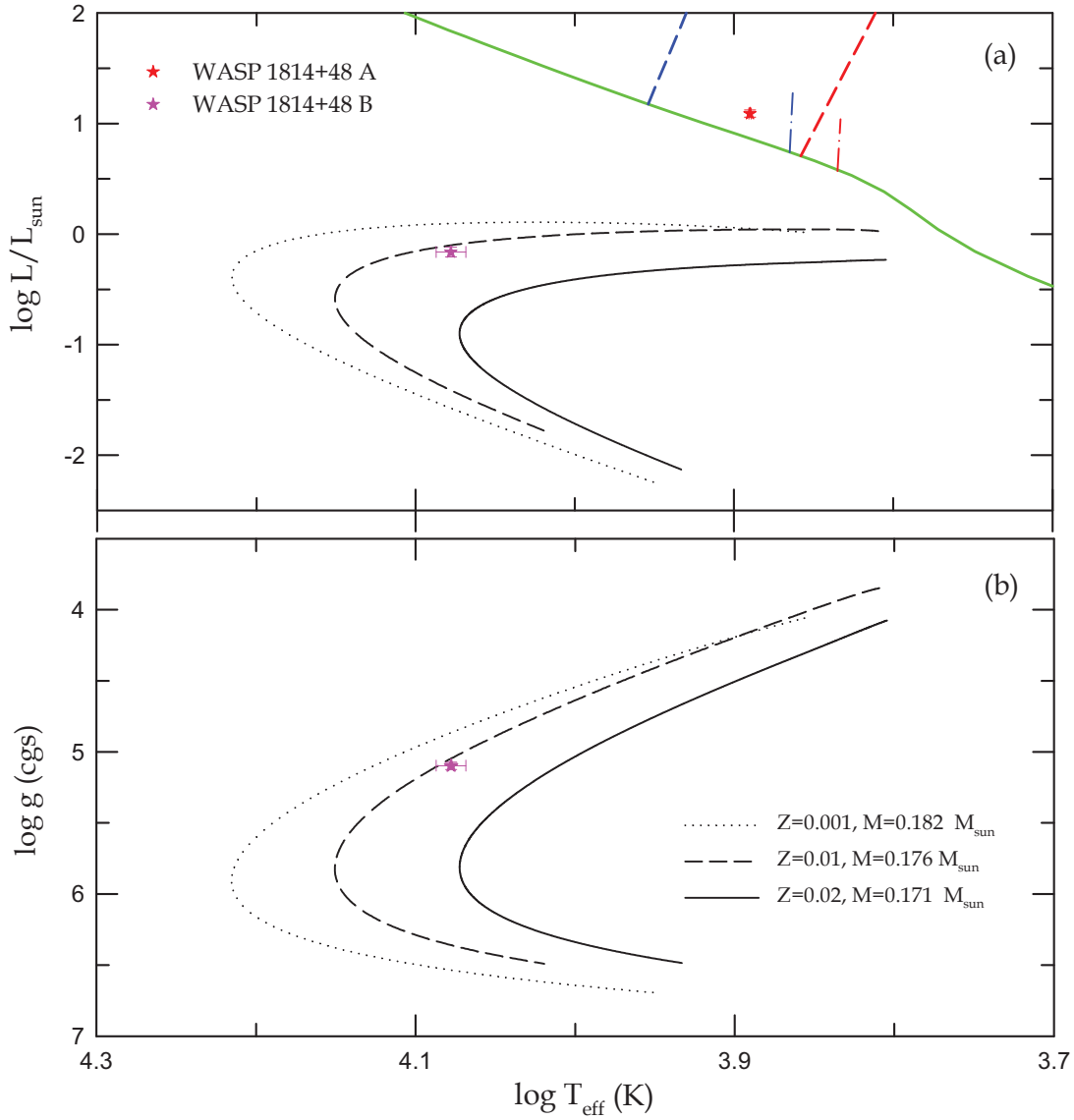


Figure 7. (a) H-R and (b) $\log T_{\text{eff}} - \log g$ diagrams for WASP 1814+48 (star symbols). In both panels, the black dotted, dashed, and solid lines are the evolutionary tracks of low-mass He WDs with metallicities Z of 0.001, 0.01, and 0.02, respectively, for masses of $0.182 M_{\odot}$, $0.176 M_{\odot}$, and $0.171 M_{\odot}$ (Istrate et al. 2016). In the upper panel (a), the green solid line denotes the ZAMS for solar metallicity, and the colored dashed and dash-dotted lines represent the instability strips of δ Sct and γ Dor stars.

Table 1. TESS Eclipse Timings of WASP 1814+48. A sample is shown here: the full version is provided as supplementary material to the online article.

BJD	Error	Epoch	$O - C$	Min
2,458,683.90998	± 0.00057	-181.5	-0.00002	II
2,458,684.81013	± 0.00016	-181.0	+0.00041	I
2,458,685.70884	± 0.00038	-180.5	-0.00060	II
2,458,686.60921	± 0.00025	-180.0	+0.00006	I
2,458,687.50768	± 0.00028	-179.5	-0.00119	II
2,458,688.40861	± 0.00019	-179.0	+0.00003	I
2,458,689.30703	± 0.00033	-178.5	-0.00127	II
2,458,690.20880	± 0.00021	-178.0	+0.00079	I
2,458,691.10946	± 0.00025	-177.5	+0.00173	II
2,458,692.00737	± 0.00029	-177.0	-0.00008	I

Table 2. Radial Velocities of WASP 1814+48 A.

BJD (2,450,000+)	V_1 (km s ⁻¹)	σ_1 (km s ⁻¹)	$O - C$ (km s ⁻¹)
7,128.2085	-33.3	0.3	-0.8
8,963.1064	-41.4	0.3	1.4
8,963.1344	-45.9	0.4	-2.2
8,963.1625	-44.1	0.4	0.4
8,963.1906	-42.5	1.0	2.7
8,963.2186	-45.3	0.3	0.3
8,963.2467	-46.0	0.3	-0.1
8,963.2748	-47.6	0.3	-1.7
8,963.3029	-43.5	1.4	2.3
8,964.0968	-6.2	0.8	0.3
8,964.1249	-4.8	1.1	1.3
8,964.1876	-6.3	0.8	-0.5
8,964.2157	-6.8	0.4	-0.8
8,964.2438	-5.9	0.7	0.5
8,964.3011	-5.4	1.2	2.3
8,968.1461	-22.2	1.2	-1.7
8,968.1742	-22.3	0.3	-0.1
8,968.2023	-24.4	0.4	0.0
9,000.2267	-7.2	0.4	-0.9
9,304.1956	-7.2	0.8	-0.8
9,304.2237	-7.2	1.1	-1.2
9,304.2518	-5.3	0.3	0.5
9,304.2799	-7.1	0.7	-1.3
9,304.3081	-5.2	0.3	0.8
9,304.3362	-4.9	0.8	1.5
9,305.1875	-42.9	0.9	2.9
9,305.2156	-47.0	1.6	-1.4
9,305.2437	-44.4	0.5	0.7
9,305.2719	-44.1	0.6	0.4
9,305.3000	-42.5	0.7	1.1
9,305.3281	-42.2	0.6	0.4

This paper has been typeset from a \TeX / \LaTeX file prepared by the author.

Table 3. Orbital Elements of WASP 1814+48.

Parameter	Value
T_0 (HJD)	$2,459,010.5067 \pm 0.0054$
P (day) ^a	1.79943078
γ (km s ⁻¹)	-25.85 ± 0.20
K_1 (km s ⁻¹)	20.17 ± 0.23
$a_1 \sin i$ (R_\odot)	0.717 ± 0.010
$f(M)$ (M_\odot)	0.00153 ± 0.00010
rms (km s ⁻¹)	1.35

^a Fixed.**Table 4.** Light and Velocity Parameters of WASP 1814+48.

Parameter	Primary	Secondary
T_0 (HJD)	$2,459,010.50670 \pm 0.00023$	
P (day)	1.7994280 ± 0.0000014	
a (R_\odot)	7.611 ± 0.095	
γ (km s ⁻¹)	-25.65 ± 0.22	
K_1 (km s ⁻¹)	20.13 ± 0.23	
K_2 (km s ⁻¹)	193.9 ± 2.7	
q	0.1038 ± 0.0019	
i (deg)	89.27 ± 0.13	
T (K)	7770 ± 130	$11,964 \pm 256$
Ω	4.041 ± 0.022	5.522 ± 0.041
Ω_{in}^a	1.971	
f (%) ^b	48.8	35.7
X, Y	0.664, 0.226	0.737, 0.075
x, y	0.506, 0.213	0.371, 0.186
$l/(l_1 + l_2)$	0.9784 ± 0.0005	0.0216
r (pole)	0.2538 ± 0.0015	0.0255 ± 0.0006
r (point)	0.2570 ± 0.0016	0.0255 ± 0.0006
r (side)	0.2561 ± 0.0016	0.0255 ± 0.0006
r (back)	0.2567 ± 0.0016	0.0255 ± 0.0006
r (volume) ^c	0.2556 ± 0.0016	0.0255 ± 0.0006

^a Potential for the inner critical Roche surface.^b Fill-out factor $f = \Omega_{\text{in}}/\Omega \times 100$.^c Mean volume radius.**Table 5.** Absolute Parameters of WASP 1814+48.

Parameter	Primary	Secondary
M (M_\odot)	1.659 ± 0.048	0.172 ± 0.005
R (R_\odot)	1.945 ± 0.027	0.194 ± 0.005
$\log g$ (cgs)	4.080 ± 0.018	5.098 ± 0.026
ρ (ρ_\odot)	0.226 ± 0.012	23.6 ± 2.0
v_{sync} (km s ⁻¹)	54.70 ± 0.77	5.46 ± 0.15
$v \sin i$ (km s ⁻¹)	47 ± 6	
T_{eff} (K)	7770 ± 130	$11,964 \pm 256$
L (L_\odot)	12.35 ± 0.90	0.69 ± 0.07
M_{bol} (mag)	2.00 ± 0.08	5.13 ± 0.11
BC (mag)	0.03 ± 0.01	-0.68 ± 0.05
M_V (mag)	1.97 ± 0.08	5.81 ± 0.12
Distance (pc)	536 ± 20	

Table 6. Results of the multiple frequency analysis for WASP 1814+48^a.

	Frequency (day ⁻¹)	Amplitude (mmag)	Phase (rad)	S/N ^b	Remark
f_1	33.70479±0.00001	0.618±0.018	3.23±0.08	59.44	
f_2	32.80546±0.00001	0.504±0.018	4.55±0.10	48.02	
f_3	0.55558±0.00003	0.221±0.026	2.44±0.34	14.62	$1f_{\text{orb}}$
f_4	1.66715±0.00005	0.136±0.024	5.43±0.52	9.61	$3f_{\text{orb}}$
f_5	1.10969±0.00004	0.156±0.025	4.48±0.47	10.58	$2f_{\text{orb}}$
f_6	32.59328±0.00005	0.104±0.018	4.36±0.51	9.92	
f_7	2.77858±0.00006	0.104±0.022	0.35±0.63	7.95	$5f_{\text{orb}}$
f_8	0.45251±0.00008	0.090±0.026	4.73±0.85	5.93	
f_9	35.86918±0.00005	0.096±0.018	1.91±0.54	9.21	
f_{10}	0.49203±0.00008	0.088±0.026	0.53±0.86	5.82	
f_{11}	33.91699±0.00005	0.091±0.018	3.67±0.58	8.59	
f_{12}	0.39523±0.00008	0.087±0.026	5.55±0.88	5.71	
f_{13}	0.50368±0.00009	0.078±0.026	1.19±0.98	5.11	
f_{14}	9.44726±0.00006	0.079±0.019	2.19±0.70	7.15	$17f_{\text{orb}}$
f_{15}	7.22447±0.00006	0.074±0.018	6.25±0.71	7.03	$13f_{\text{orb}}$
f_{16}	8.33590±0.00006	0.074±0.018	5.07±0.72	6.98	$15f_{\text{orb}}$
f_{17}	0.47818±0.00008	0.083±0.026	4.40±0.91	5.49	
f_{18}	0.93935±0.00011	0.061±0.025	3.36±1.19	4.21	
f_{19}	1.11036±0.00005	0.129±0.025	4.06±0.57	8.72	$2f_{\text{orb}}$
f_{20}	0.23589±0.00010	0.069±0.026	3.84±1.12	4.48	
f_{21}	3.89005±0.00008	0.063±0.020	4.52±0.94	5.32	$7f_{\text{orb}}$
f_{22}	0.98233±0.00011	0.064±0.026	5.72±1.18	4.26	$2f_{10}$
f_{23}	3.33800±0.00009	0.062±0.021	1.47±1.01	4.96	$6f_{\text{orb}}(?)$
f_{24}	1.23523±0.00011	0.063±0.026	4.96±1.21	4.13	$2f_5 - f_{22}$
f_{25}	0.29531±0.00011	0.061±0.026	3.10±1.26	3.99	
f_{26}	0.34236±0.00010	0.067±0.026	1.22±1.14	4.41	
f_{27}	2.22238±0.00011	0.056±0.023	4.33±1.23	4.08	$4f_{\text{orb}}$
f_{28}	10.00365±0.00010	0.051±0.019	2.32±1.12	4.47	$18f_{\text{orb}}$
f_{29}	8.89224±0.00010	0.050±0.019	2.22±1.09	4.58	$16f_{\text{orb}}$
f_{30}	10.55889±0.00010	0.049±0.020	2.51±1.17	4.30	$19f_{\text{orb}}$
f_{31}	11.11509±0.00011	0.048±0.020	2.89±1.20	4.17	$20f_{\text{orb}}$
f_{32}	43.34495±0.00009	0.047±0.017	0.48±1.04	4.82	
f_{33}	28.89502±0.00010	0.047±0.018	4.15±1.12	4.49	$f_{32} - 26f_{\text{orb}}$
f_{34}	16.11616±0.00010	0.046±0.017	5.67±1.09	4.60	$29f_{\text{orb}}$
f_{35}	26.67267±0.00011	0.045±0.018	4.20±1.19	4.20	$f_{32} - 30f_{\text{orb}}$
f_{36}	4.45508±0.00011	0.045±0.019	2.07±1.27	3.96	
f_{37}	18.89540±0.00010	0.045±0.017	2.30±1.10	4.55	$34f_{\text{orb}}$
f_{38}	21.12724±0.00010	0.044±0.017	6.11±1.10	4.56	
f_{39}	203.85745±0.00010	0.044±0.017	1.85±1.13	4.43	
f_{40}	15.00015±0.00011	0.042±0.018	5.37±1.23	4.07	$27f_{\text{orb}}(?)$
f_{41}	23.84905±0.00011	0.042±0.018	2.34±1.23	4.09	
f_{42}	128.93254±0.00011	0.042±0.017	1.40±1.19	4.22	
f_{43}	31.57909±0.00011	0.042±0.018	3.19±1.25	4.00	
f_{44}	22.78744±0.00011	0.042±0.017	3.01±1.21	4.16	$41f_{\text{orb}}(?)$
f_{45}	135.25945±0.00011	0.041±0.017	3.53±1.22	4.11	
f_{46}	36.54663±0.00011	0.041±0.018	1.60±1.25	4.02	
f_{47}	23.33990±0.00011	0.041±0.017	1.90±1.23	4.07	$42f_{\text{orb}}$
f_{48}	287.85952±0.00011	0.041±0.017	3.45±1.18	4.24	
f_{49}	17.78415±0.00011	0.041±0.017	6.20±1.22	4.12	$32f_{\text{orb}}$
f_{50}	42.23532±0.00011	0.041±0.017	0.07±1.22	4.12	$f_{32} - 2f_{\text{orb}}$
f_{51}	200.42459±0.00010	0.040±0.016	2.74±1.18	4.26	
f_{52}	20.00649±0.00011	0.040±0.016	3.73±1.20	4.18	$36f_{\text{orb}}$

^a Frequencies are listed in order of detection.^b Calculated in a range of 5 day⁻¹ around each frequency.